inventions

MDPI

Article

Experimental Investigation on the Effect of Size and Pitch of Hydrophobic Square Patterns on the Pool Boiling Heat Transfer Performance of Cylindrical Copper Surface

Sujith Kumar C. S., Yao Wen Chang, Mario R. Mata Arenales, Long-Sheng Kuo, Yu Hsuan Chuang and Ping-Hei Chen *

Department of Mechanical Engineering, National Taiwan University, Taipei 10617, Taiwan; sujithdeepam@gmail.com (S.K.C.S.); steven84@livemail.tw (Y.W.C.); mr.mariomata@gmail.com (M.R.M.A.); d94522017@ntu.edu.tw (L.-S.K.); R05522121@ntu.edu.tw (Y.H.C.)

* Correspondence: phchen@ntu.edu.tw

Received: 2 February 2018; Accepted: 6 March 2018; Published: 8 March 2018

Abstract: In this work, pool boiling heat transfer tests were conducted for investigating the effects of the size and pitch of the hydrophobic square patterns on a copper test piece with the following dimensions: 40 mm long, 25 mm outer diameter, and 18 mm inner diameter. The size of the square patterns and the pitch were varied with an increment of 0.5 mm from 1 mm to 3 mm and from 4.5 to 5.5 mm, respectively. Among the various square patterns of different size and pitch, the 2 mm size square pattern with 5 mm pitch (inter-distance 3 mm) was found to be the best because it gives the advantage of bubble coalescence behavior and also the rewetting phenomenon. The observed bubble departure diameter was 2.35 mm, and using this diameter, we predicted the maximum inter-distance between the patterns for producing inter coalescence of bubbles in the axial direction was 3.12 mm. Therefore, a side-by-side distance of 3 mm, which was closed to the estimated inter-distance graphically, can avoid the earlier inter coalescence of the bubbles between patterns on the surface in the axial direction. This results in better pool boiling heat transfer performance. Highlights: (1) Heterogeneous wettable structures were obtained on the copper surface using screen printing techniques; (2) The effect of the size and pitch of the hydrophobic patterns on the bubble dynamics was determined; (3) The wall superheats of all the heterogeneous wettable surfaces were less than the plain copper surface; (4) The highest heat transfer coefficient was obtained from the hydrophobic pattern with 2 mm size and 5 mm pitch.

Keywords: pool boiling; heterogeneous wettable surface; screen printing; boiling heat transfer coefficient; bubble dynamics

1. Introduction

Phase change heat transfer systems, such as pool and flow boiling heat sinks, are used extensively in the fields of refrigeration, air conditioning, and electronic devices cooling [1–3]. During the boiling heat transfer, the working fluid can absorb a large amount of heat with a small wall superheat due to its large latent heat of vaporization [4,5]. The effectiveness of the boiling heat transfer is mostly determined by the limiting parameters like critical heat flux (CHF) and the onset of nucleate boiling (ONB). The higher CHF and the earlier ONB are desirable for better performance. Extensive research works have been carried out for improving boiling heat transfer performance, and they are generally classified into active, passive, and compound techniques [6]. The passive heat transfer enhancement techniques are usually used for improving the boiling heat transfer performance, because by using

this technique, better heat transfer performance can be achieved without any external power supply. Usually, many passive techniques are used to improve the pool boiling heat transfer performance, such as increasing the degree of subcooling, improving the fluid's physical properties by adding nanoparticles, surface modification, and surface coating [7–10].

Surface wettability has an important role in the enhancement of the pool boiling performance, due to its dependence on the bubble departure frequency. Based on the relationship between the bubble departure phenomenon and free convection, the bubble departure frequency is (f_e) calculated using the Equation (1), which is inversely proportional to the duration of bubble growth (t_g) and the time interval between the departure of a bubble and appearance of the next bubble (t_w) [11].

$$f_e = \frac{1}{t_g + t_w} \tag{1}$$

The bubble growth time will increase with the increase in departure diameter. A smaller diameter leads to better pool boiling performance due to the high departure frequency [11]. In 1935, Fritz proposed a correlation for the departure diameter by considering the wettability effect, which is shown in Equation (2) [12].

$$\mathrm{D}_d = 0.626997 \varnothing \left[\frac{\gamma}{\mathrm{g}\,(\rho_L - \rho_G)} \right]^{0.5} \tag{2}$$

where D_d is the departure diameter, $\varnothing$ is the receding contact angle, γ is the surface tension, g is the acceleration due to gravity, and ρ_L and ρ_G are the liquid and vapor density, respectively.

The large contact angle of the hydrophobic surface gives a higher departure diameter, resulting in more bubble growth time. However, some part of the departing bubble remains on the surface for the continuous generation of bubbles without any waiting time [13]. The continuous generation of the bubbles on the hydrophobic surface stops the rewetting of liquid, causing deterioration of boiling heat transfer. This results in the early dry out of the surface, therefore, the use of biphilic surfaces with mixed wettability gives the ideal performance at all regimes of boiling. This is due to the early ONB facilitated by the hydrophobic dots, reduction in the size of the generated bubbles, and prevention of the earlier vapor dry out [14].

Various techniques are available for producing the heterogeneous wettable (biphilic) surface, such as the laser jet printing, photolithography, and screen printing [13–16]. Among them, the screen printing technique is the best one, as this technique offers a number of advantages compared to the others, namely, scalability of the process, cost-effectiveness with regard to equipment costs and energy needs, and ease of operation (either on a flat or a curved surface).

Only a few works have investigated the effect of size and pitch of patterns on pool boiling heat transfer performance on the cylindrical surface. In this study, the screen printing technique was used to produce the heterogeneous wettable surface. Five different size square patterns with the constant pitch of 5 mm and three different pitch square patterns with the constant size of 2 mm were prepared by printing the hydrophobic polymer composite on the plain copper surface. Subsequently, the pool boiling performances of the prepared heterogeneous wettable surfaces were compared with the plain copper surface.

2. Experimental Process

2.1. Surface Modification

2.1.1. Copper Test Piece Cleaning Procedure

A hollow copper cylinder of the dimensions shown in Figure 1b was selected as the test piece. Before the surface coating, the copper test piece was polished with #2000 emery paper for removing the free oxide layer from the surface. Then, the copper was rinsed with acetone followed by de-ionized (DI) water. After that, the test piece was placed in an oven maintained at 120 °C for 2 h [15].

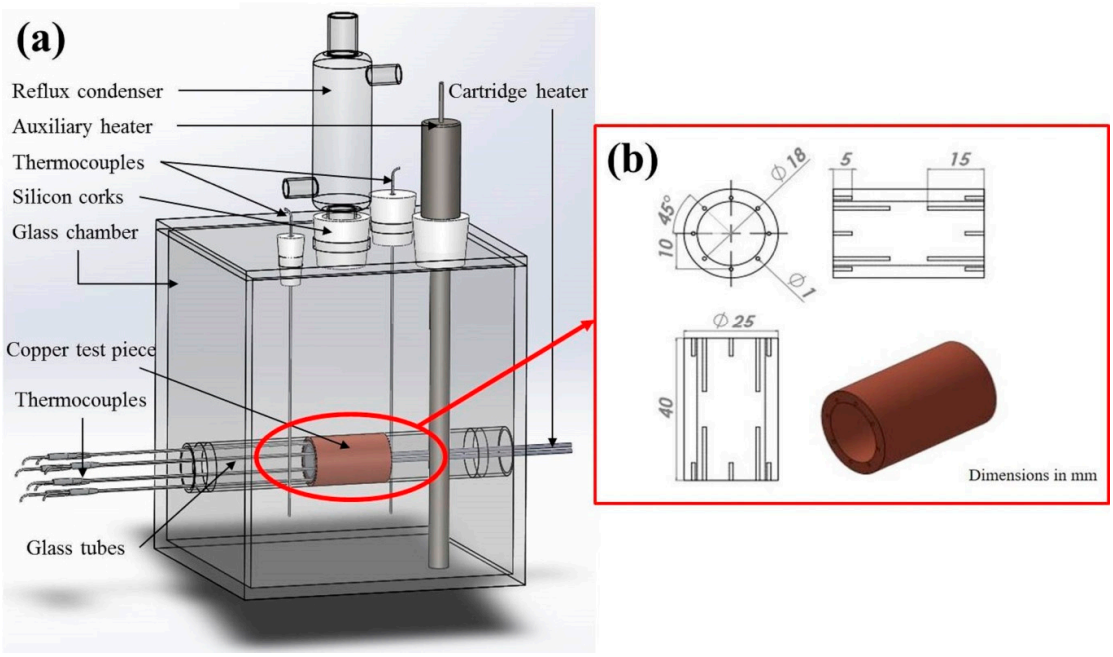

Figure 1. (**a**) Assembled view of the test section and (**b**) dimensional details of the copper test piece.

2.1.2. Preparation of the Polymer Mixture for Screen Printing

In this work, we used polymethyl methacrylate (PMMA) resin as the paint, epoxy as the hardener, and Trichloro (1H, 1H, 2H, 2H-perfluorooctyl) silane as the hydrophobic agent. The hydrophobic polymer mixture for printing was prepared by mixing 4 g of PMMA with 1 g of epoxy for 2 min and then adding 1 mL of Trichloro (1H, 1H, 2H, 2H-perfluorooctyl) silane to the mixture and again mixing it for 2 min.

2.1.3. Preparation of the Heterogeneous Wettable Surfaces with Various Sized and Pitched Square Patterns

The fabrication process of the heterogeneous wettable surfaces on the test piece was conducted in the order shown in Figure 2a. The heterogeneous wettable surfaces with different sizes of patterns were produced by printing the polymer mixture on a cylindrical surface using the different stencil meshes. The design details of different patterns are shown in Figure 2b.

2.2. Test Section

The constructional details and important components of the test section are shown in Figure 1a. The pool boiling chamber was made with four glass side plates, one bottom glass plate, and one top polycarbonate plate. The dimension of the chamber was fixed as 140 $\times$ 140 $\times$ 160 mm. The copper test piece was fixed into the holes on the sidewalls by using two glass tubes as represented in Figure 1a. A cartridge heater of 550 W capacity was placed in the hollow test piece using the thermal paste. Eight T-type thermocouples were placed in the equally spaced 1 mm diameter holes, with alternate depths of 5 mm and 15 mm circumferentially. A Reflux condenser, an auxiliary heater, and two T-type thermocouples for measuring the bulk fluid temperature were fixed into the holes provided on the top cover by using the silicon corks [15].

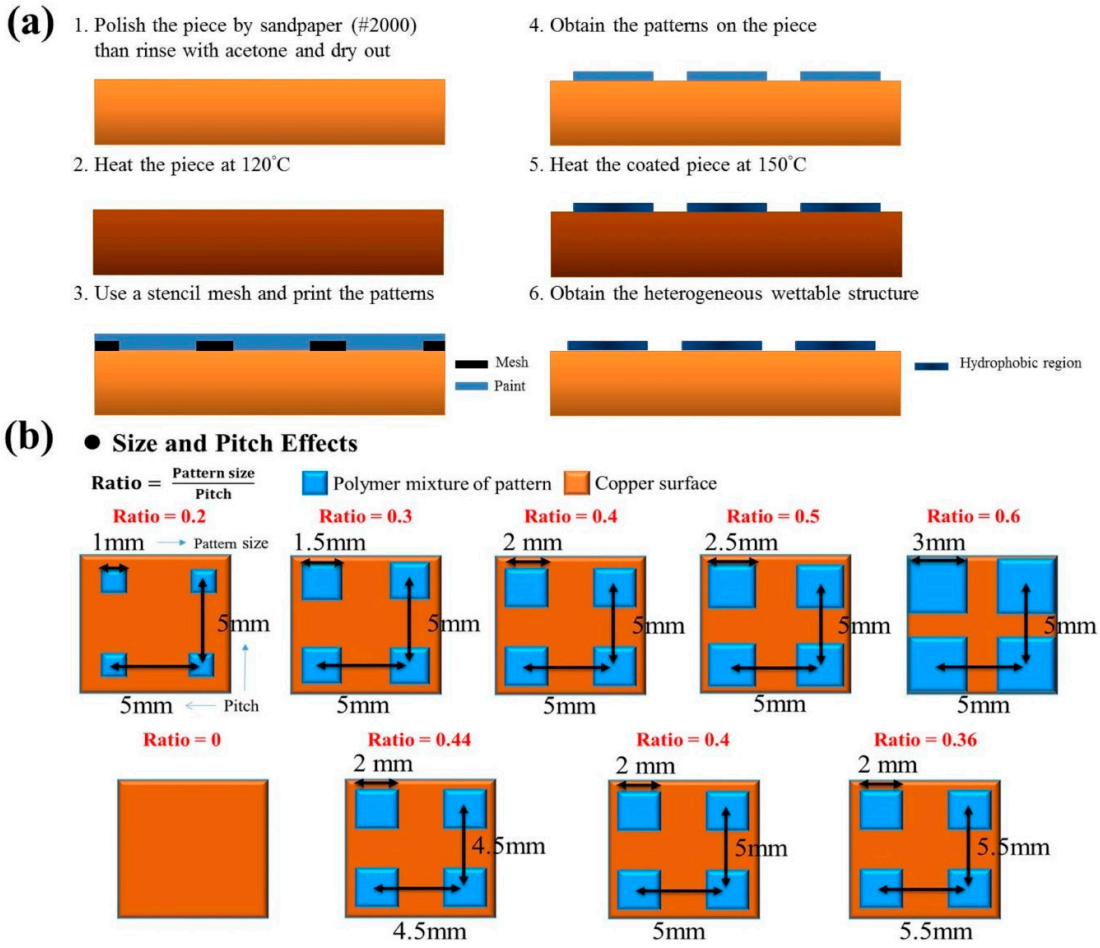

Figure 2. (**a**) Fabrication process for the heterogeneous wettable surface and (**b**) design details of different square patterns.

2.3. Experimental Setup

Figure 3 shows the annotated photograph of the experimental setup, and the important components are the tested section, DC power supply, auto transformer, chiller unit (Model: B402L; CCTCL, Taipei, Taiwan), high speed camera (Model: HSP 130; Whited Co., Taipei, Taiwan), data logger, and computer. All pool boiling heat transfer experiments were conducted at the saturated temperature and atmospheric pressure, using DI water as the working fluid. The chiller unit was used to condense the water vapor in the reflux condenser. The input power to the cartridge and auxiliary heaters were controlled by using the DC power supply (Model: GPR-20H50D; Gwinstek, Taipei, Taiwan) and autotransformer, respectively. The MX-100 data logger (Yokogawa, Taipei, Taiwan) was used for acquiring the temperature by connecting it with all thermocouples, and a high speed camera (Model: HSP 130) was used to study the bubble dynamics [15].

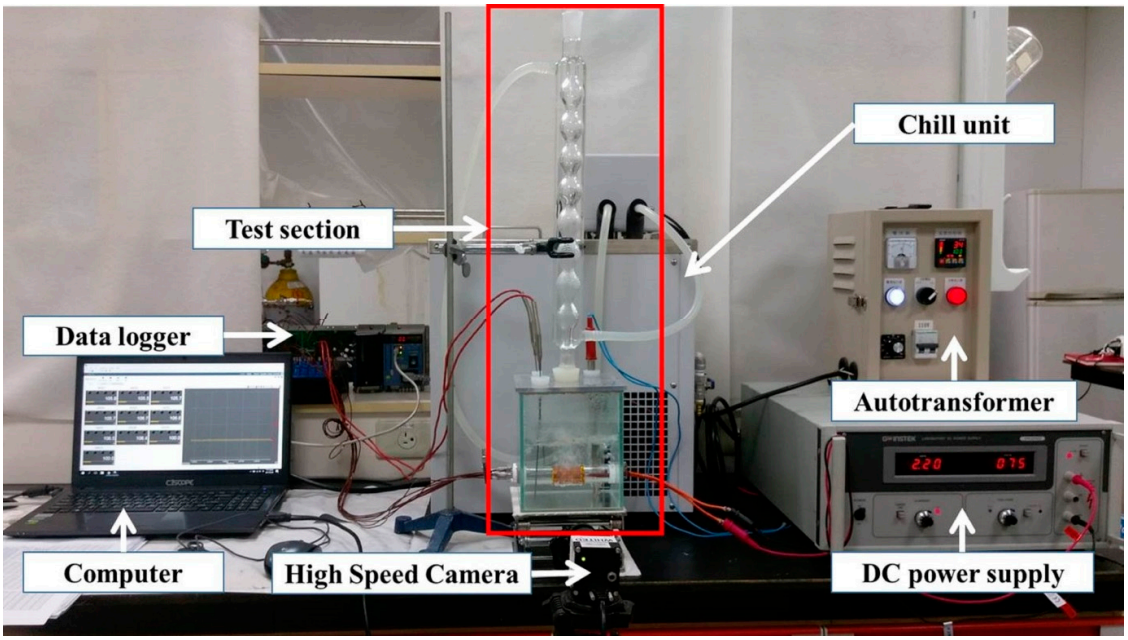

Figure 3. Annotated photograph of experimental setup.

2.4. Experimental Procedure

For obtaining the accurate, saturated pool boiling data, prior to the experiment, dissolved gas from the working fluid (DI water) was removed by vigorous boiling. After that, the reflux condenser was connected to the chiller unit which was maintained at 5 °C. The bulk temperature of the working fluid was maintained at a saturated condition using an auxiliary heater. Then, the experiment was started at an initial current of 0.1 A and we waited for 2 min to attain the steady state condition. Then, the temperature data from the thermocouples and bubble dynamics were recorded by using the data logger and the high speed camera, respectively. After that, the input current to the cartridge heater was increased with an increment of 0.3 A (during which time the voltage was found to increase), and the entire measurement procedure was repeated. The pool boiling experiment was conducted up to the maximum input current of 4 A [15].

2.5. Data Reduction and Uncertainty Analysis

The input power supplied (Q) to the cartridge heater was calculated by using the following Equation (3):

$$Q = IV \tag{3}$$

where I and V are the input current in amps and the voltage in volts, respectively.

The axial heat loss (Q_{loss}) from the two side surfaces was estimated by using Equation (4) [15,17]:

$$Q_{loss} = 2 \times k \times \left[\frac{(T_{15\ mm} - T_{5\ mm})}{\Delta x} \right] \times A_c \tag{4}$$

where k is the thermal conductivity of copper, T_{15} mm and T_5 mm are the average temperatures at depths of 15 mm and 5 mm, respectively, Δx is the difference in the depth, and A_c is the cross-section area of the test piece.

The heat flux (q'') to the boiling surface of the test piece was calculated by using the following Equation (5) [15,17]:

$$q'' = \frac{Q - Q_{loss}}{A} \tag{5}$$

where A is represented as the circumferential area of the test piece.

The wall superheat (ΔT_w) was estimated by extrapolating the average temperature T_m using the Equation (6) [15,17]:

$$\Delta T_w = T_m - \left[\frac{Q - Q_{loss}}{2\pi Lk}\right] \times \ln\left(\frac{r_o}{r_m}\right) - T_{sat} \quad (6)$$

where T_m is the average of T_{15} mm and T_5 mm, L is the length of the test piece, r_o is the outer radius of the test piece, r_m is the radius of the test piece at the measuring holes, and T_{sat} is the saturation temperature of DI water. Consequently, boiling Heat Transfer Coefficient (HTC (h)) was calculated by using the following Equation (7) [15,17]:

$$h = \frac{q''}{\Delta T_w} \quad (7)$$

The experimental uncertainties of the heat flux, wall superheat, and HTC were calculated by using the Equations (8) and (9) [18].

$$\delta q'' = \sqrt{(\delta x)^2 + \cdots + (\delta z)^2 + (\delta u)^2 + \cdots + (\delta w)^2} \left(\text{if} q'' = x + \cdots + z - (u + \cdots + w)\right) \quad (8)$$

$$\frac{\delta q''}{q''} = \sqrt{\left(\frac{\delta x}{x}\right)^2 + \cdots + \left(\frac{\delta z}{z}\right)^2 + \left(\frac{\delta u}{u}\right)^2 + \cdots + \left(\frac{\delta w}{w}\right)^2} \left(\text{if} q'' = \frac{x \times \cdots \times z}{u \times \cdots \times w}\right) \quad (9)$$

where $\delta q''$ is the uncertainity in heat flux and x, z, u, and w are the paramters used for the heat flux measurent and δx, δz, δu, and δw are its corresponding error values.

The maximum uncertainty for the heat flux, wall superheat, and HTC were found to be $\pm$15.66%, $\pm$15.80%, and $\pm$22.25%, respectively.

3. Experimental Results and Discussion

Prior to the heat transfer performance analysis, the dynamic contact angles of the surfaces were measured using the contact angle goniometer (Model 100 SB; Sindatek, Taipei, Taiwan). Supplementary videos show the advancing and the receding contact angles of the plain copper surface and the hydrophobic surface (Supplementary videos: video S1, video S2, video S3, and video S4 and descriptions). The average values of the advancing and the receding contact angles of the plain copper and the hydrophobic patterns are shown in Table 1. The average surface roughness values of the plain copper and the hydrophobic patterns were measured using a probe type surface roughness analyzer (Model ET 400; Kosaka Laboratory Ltd., Tokyo, Japan) and the corresponding values were 0.037 μm and 0.323 μm, respectively [19].

Table 1. Advancing and receding contact angles of the plain copper surface and the hydrophobic surface.

	Advancing Contact Angle (°)	Receding Contact Angle (°)
Plain copper surface	104.79	3.22
Hydrophobic surface	124.32	54.79

Pool boiling experiments were conducted using DI water as the working fluid, and the fluid was maintained at the saturated conditions. In this section, the effects of size and pitch of the patterns on the pool boiling heat transfer performance are investigated. Subsequently, the results were analyzed by using the bubble departure behaviors and the obtained temperatures. The details of various test surfaces selected for the pool boiling heat transfer studies are given in Table 2.

Table 2. Sample information.

Aspect Ratio	Size (mm)	Pitch (mm)	Number of Patterns	Area Ratio (%)
Case: Various sizes of pattern				
0.20	1.0	5.0	105	3.34
0.30	1.5	5.0	105	7.52
0.40	2.0	5.0	105	13.37
0.50	2.5	5.0	105	20.89
0.60	3.0	5.0	105	30.08
Case: Various pitches of pattern				
0.36	2.0	5.5	98	12.48
0.40	2.0	5.0	105	13.37
0.44	2.0	4.5	136	17.32
Definition aspect ratio = the size of pattern/pitch between the pattern Definition of area ratio = total area of hydrophobic patterns/heating area				

3.1. Bubble Dynamics

It is quite important to understand the bubble developing behaviors because the enhancements in the heat transfer performance highly depend on the bubble dynamics. Firstly, the bubble developing behaviors are studied using the schematic drawings shown in Figures 4 and 5. Mainly, three types of the bubble development behaviors were observed during the pool boiling experiments: the isolated development of a bubble, the internal coalescence of bubbles on a pattern, and the inter coalescence of bubbles between the adjacent patterns (axial and circumferential directions). The bubble development phenomenon was accompanied by nucleation, growth, and departure on the heated surface, therefore, the bubble departure time is the time for the entire process of bubble development. The schematic representation of the isolated development of the bubbles is shown in Figure 4a. This type of development produces a longer departure time as compared to that the others, due to the phenomenon of bubble coalescences not occuring during the development [19]. This type of bubble development behavior was, usually, found at low heat fluxes. On the other hand, at high heat fluxes, the phenomenon of bubble coalescence occurred predominately. The internal coalescence of bubbles (Figure 4b), described as the merging of the bubbles, took place on the same pattern. Moreover, the inter coalescence of bubbles, described as the merging of bubbles between the neighboring patterns, was found in the circumferential and axial direction (Figures 4c and 5a,b). Circumferential inter coalescence happened due to the cylindrical nature of the test piece. This phenomenon happened due to the merging of bubbles during departure of one bubble from the bottom pattern to one formed on the pattern on top of it. During the circumferential inter coalescence, no shift on the contact line of the formed bubble was found. Consequently, this phenomenon has a shorter departure time owing to the influence of bubble coalescence [20]. However, in the axial direction, coalescence depends on the side-by-side distance between the patterns. As represented in Figure 5a, small pitch (small side-by-side distance) led to more chances of earlier inter coalescence of bubbles during the development of bubbles in the axial direction. This created a shift in the contact line and, thereby, produced more intermediate resistance between the bubble and the surface, due to the increase in the contact area and the time. On the other hand, as shown in Figure 5b, if the side-by-side distance was sufficiently higher, then the earlier coalescence of bubbles, and subsequent shift in the contact line, can be avoided, resulting in lower intermediate resistance [20].

The effects of pattern sizes and pitches on the number of active sites and their location are investigated using the Figure 6. As represented in the Figure 6, when the aspect ratios are 0.2 and 0.4, the active nucleation sites were found only on the interfaces between the pattern and its surrounding, but for the other two aspect ratios, the nucleation sites were also observed in the space between the patterns. The 0.4 aspect ratio surface produced more numbers of nucleation sites as compared to that

of the other surfaces. The 0.6 and 0.44 aspect ratio surfaces also produced nucleation sites between the patterns due to the higher local surface temperature created because of the insufficient rewetting action.

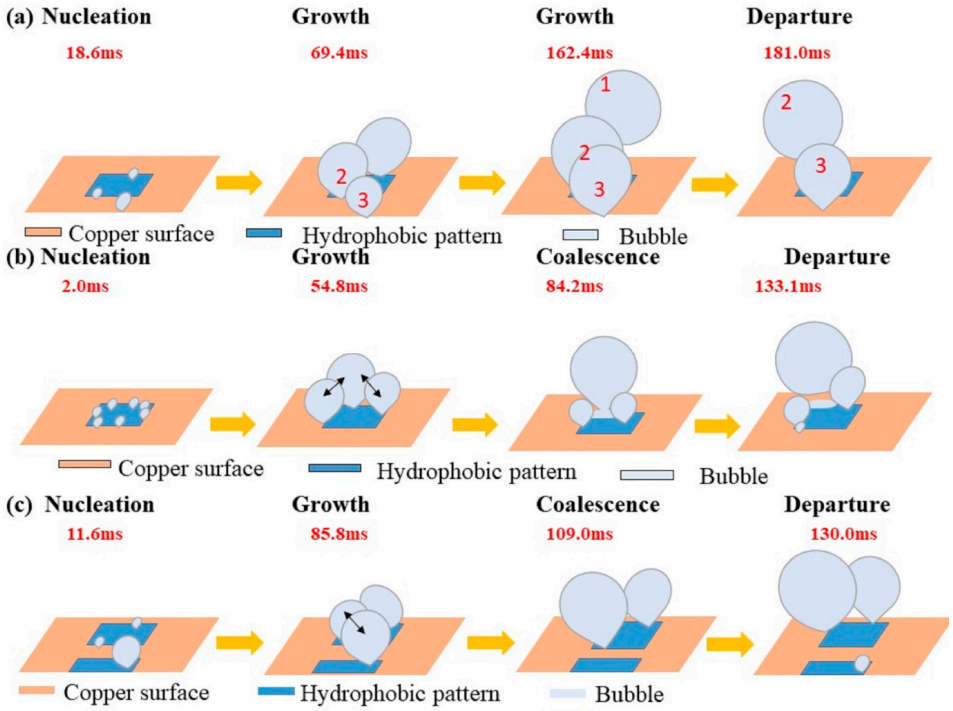

Figure 4. Schematic of different bubble development mechanisms at a constant heat flux of 7 kW/m^2 (**a**) isolated development of bubble; (**b**) internal coalescence of bubbles on a pattern; (**c**) inter coalescence of bubbles on the neighboring pattern in circumferential direction.

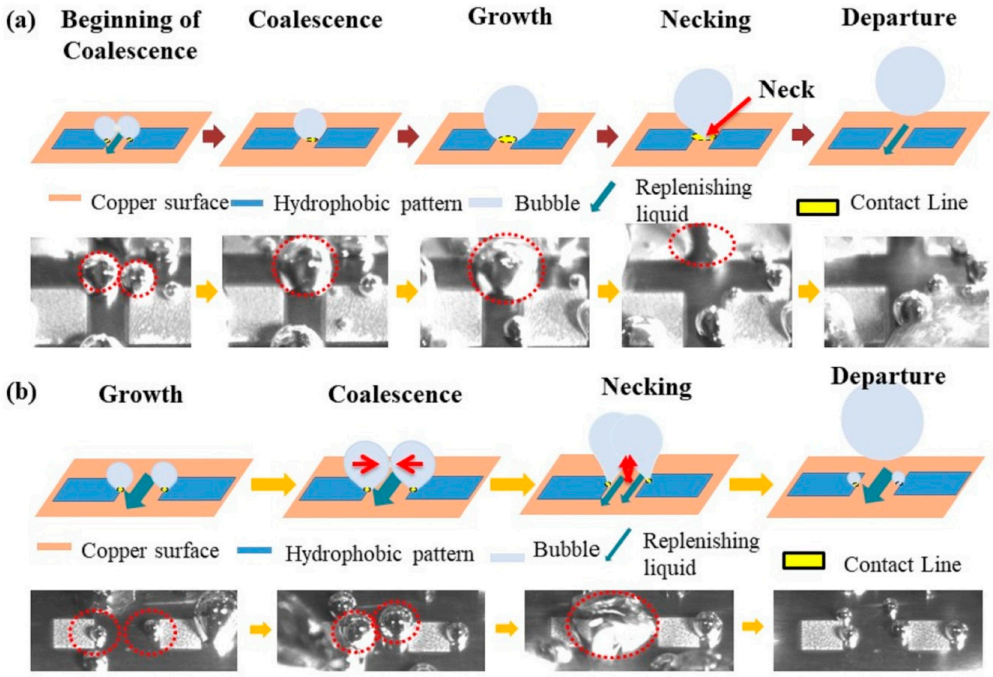

Figure 5. Bubble merging mechanism in axial direction (**a**) earlier inter coalescence of bubbles and (**b**) inter coalescence of bubbles after their isolated development, at a constant heat flux of 7 kW/m^2.

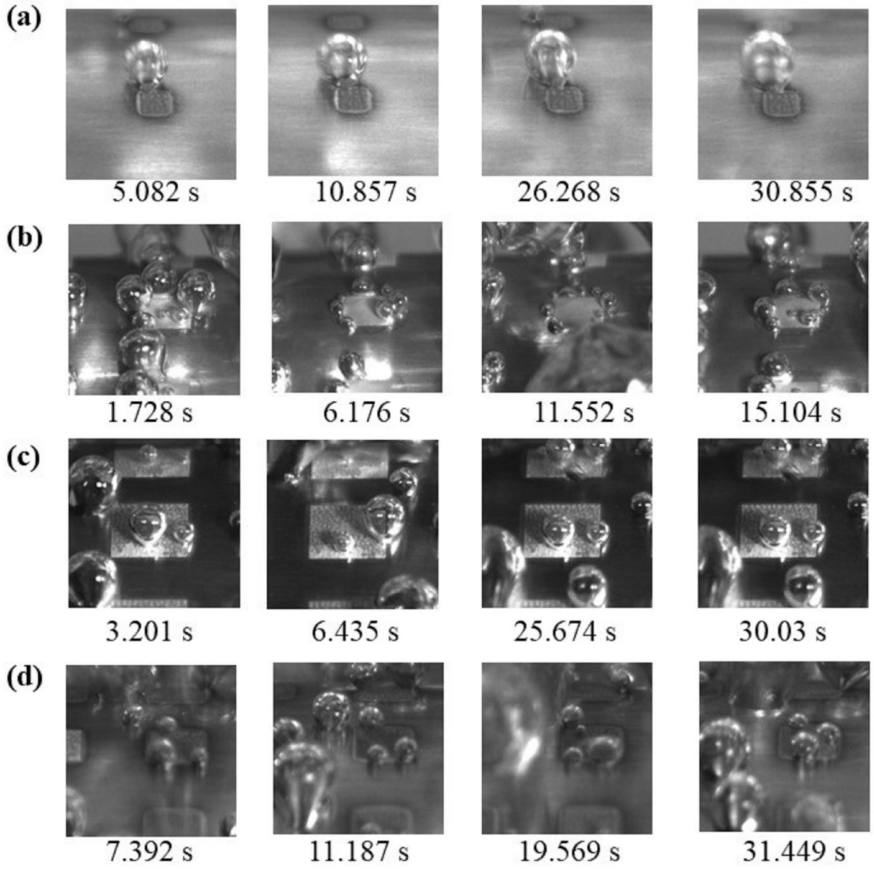

Figure 6. Comparison of the number of active nucleation sites for the surfaces with (**a**) 0.2 aspect ratio; (**b**) 0.4 aspect ratio; (**c**) 0.6 aspect ratio; and (**d**) 0.44 aspect ratio, at a constant input power of 30 W.

In addition, the bubble departure behaviors were investigated in this work. Figure 7 indicated that the bubble formed with a balloon-like shape, which had a point contact with the surface due to the necking effect [13], resulted in an easy departure. During the merging, bubbles covered the pattern partially; therefore, the remaining area would act as the nucleation site for the new bubbles.

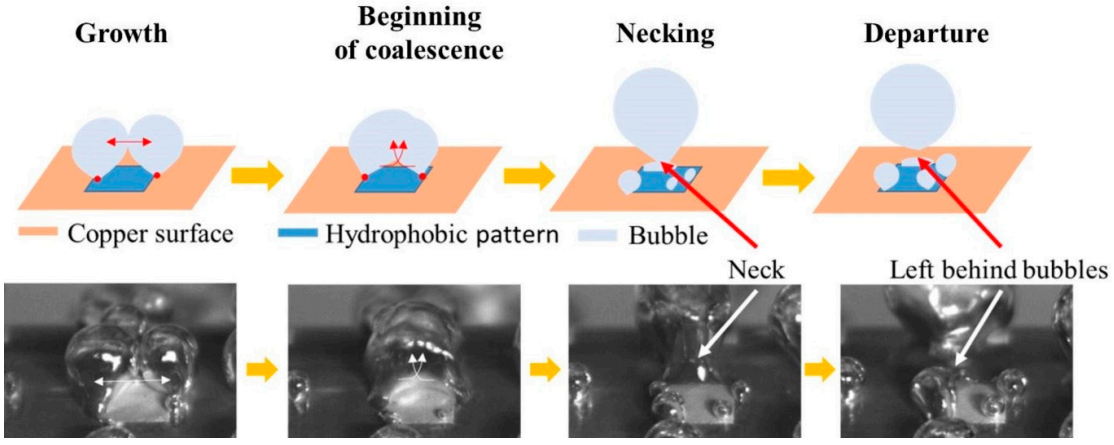

Figure 7. Bubble departure behavior of the pattern (ratio = 0.4) at the heat flux of 7 kW/m^2.

3.2. Pool Boiling Heat Transfer Performance

Figure 8 demonstrates the pool boiling curves of the plain copper surface (Ratio = 0) and the five biphilic surfaces with different sized patterns. According to the test results, the pool boiling curves of the surfaces with various sizes of the patterns are shifting towards the left as compared to the plain surface (Ratio = 0), resulting in an improvement in the pool boiling heat transfer performance. This is due to the early ONB on the hydrophobic patterns and the higher rate of coalescence. In addition, the most leftward shift in the pool boiling curve happened for the 2 mm sized square patterned surface (Ratio = 0.4), however, the 1 mm sized square patterned surface (Ratio = 0.2) produced the minimum shift. The results of the square patterns of 1.5 mm (Ratio = 0.3) and 3 mm (Ratio = 0.6) are close to each other. However, the pool boiling curve of the 2.5 mm sized square pattern (Ratio = 0.5) shows a slight leftward shift compared to the other two (1.5 mm (Ratio = 0.3) and 3 mm (Ratio = 0.6)). The 2 mm sized square pattern gives the lowest wall superheat for all heat fluxes, which results in higher HTCs. Furthermore, Figure 9a expresses that the peak value of the HTC takes place at the aspect ratio of 0.4 (2 mm square pattern). Moreover, this aspect ratio expressed the highest HTCs for every specific heat flux. Figure 9b shows the enhancement percentages of all aspect ratio surfaces compared with the plain surface (Ratio = 0); they are reduced with an increase in heat fluxes.

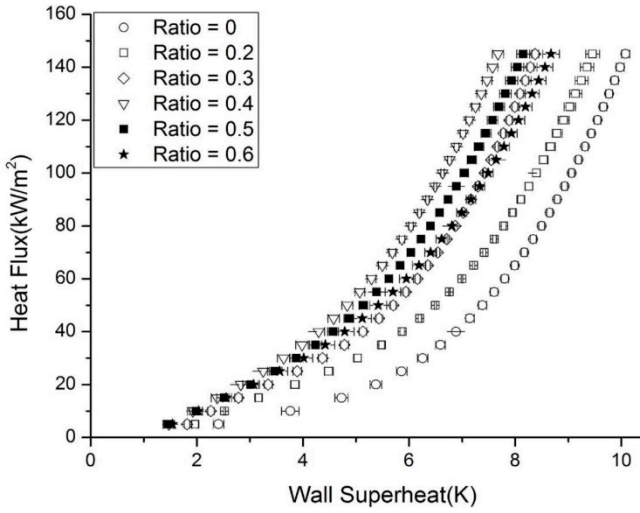

Figure 8. The effect of the pattern size on the pool boiling curves of the various tested surfaces.

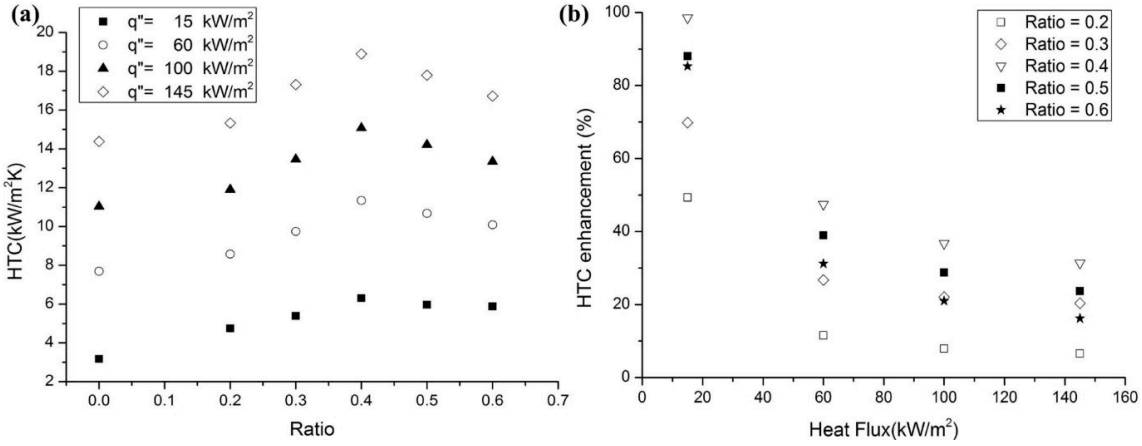

Figure 9. The effect of the pattern size on (**a**) the HTC values for the specific heat fluxes and (**b**) the enhancement percentage in HTC with respect to the heat flux.

The bubble dynamic behavior is a key factor to understanding the results obtained from the pool boiling experiments. Initially, because of the hydrophobic patterns, many bubbles formed early on the tested pieces, leading to a higher HTC at low heat fluxes as compared to that of the Surface-P (Ratio = 0). However, the number of activation sites and the bubble coalescence phenomena are different in each case. The 1 mm sized square pattern (Ratio = 0.2) only shows the internal coalescence on the patterns because the inter-distance between two patterns is too large to cause the inter coalescence of the bubbles (Figure 10a). In addition, the number of active nucleation sites is low compared to the other surfaces. The same situation of bubble coalescence happens on the 1.5 mm pattern (Ratio = 0.3), however, it produces better results due to the presence of more nucleation sites on the hydrophobic patterns (Figure 10b). While on the 2 mm pattern (Ratio = 0.4), both the higher number of active nucleation sites and bubble coalescences (internal and inter) found on the heated surface result in the best boiling heat transfer performance (Figure 10c). However, the 2.5 mm pattern (Ratio = 0.5) produces lower heat transfer performance due to the slowing down of the rewetting action and bubble formation on the plain areas. The insufficient side-by-side distance led to early coalescences of bubbles in the axial direction as mentioned in Figure 5a. During the merging of bubbles, usually the contact line moves between the patterns and that disturbs the flow of replenishing liquid from the surroundings (Figure 10d). Therefore, as the square pattern size increases to 3 mm (Ratio = 0.6), the problem of rewetting will occur more seriously, even though both types of bubble coalescences still show up on the heated surface (Figure 10e). Therefore, pool boiling performance depends on both bubble dynamics and the rewetting action of fluid towards the surface [20].

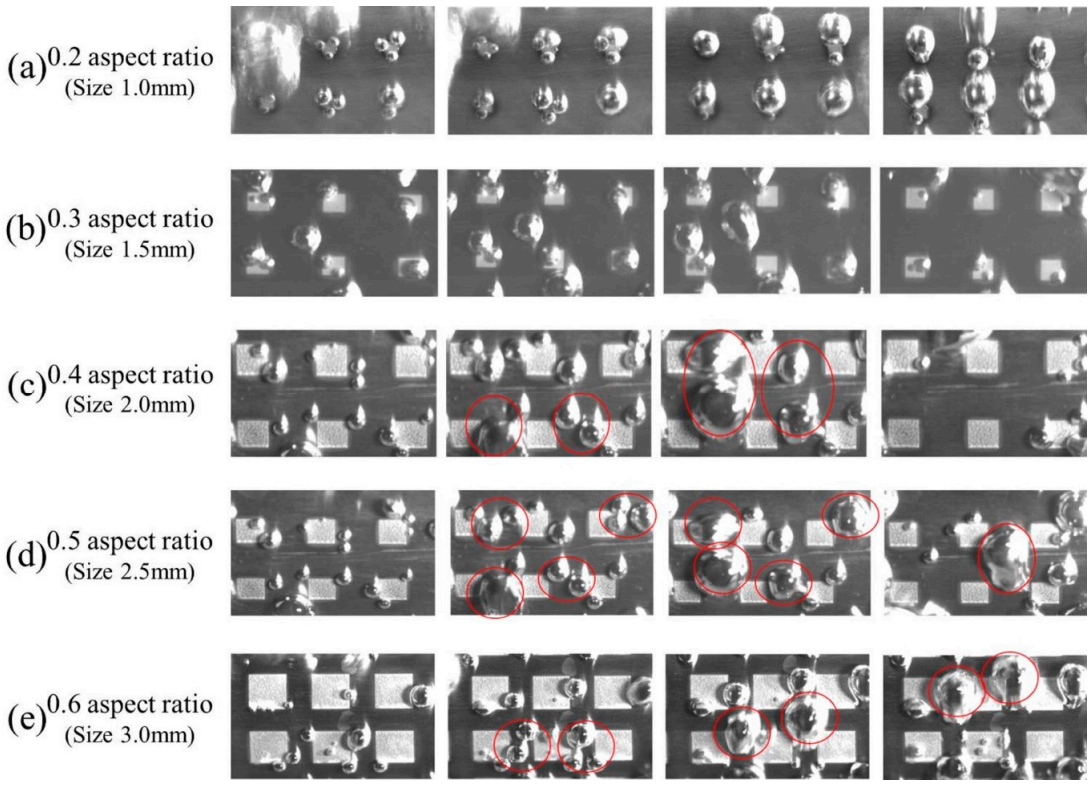

Figure 10. Bubble development mechanisms of the surfaces with (**a**) 0.2 aspect ratio; (**b**) 0.3 aspect ratio; (**c**) 0.4 aspect ratio; (**d**) 0.5 aspect ratio; and (**e**) 0.6 aspect ratio.

In order to identify the effect of the pitch on the pool boiling heat transfer, the size of the square patterns was fixed to 2 mm and the pitch was varied from 4.5 to 5.5 mm. Figure 11 represents the effect of various pitches on pool boiling performance. Both cases, the pitch = 5.5 mm (Ratio = 0.36) and 4.5 mm (Ratio = 0.44), produce close boiling curves. However, the result for the pitch = 5 mm

(Ratio = 0.4) is the most leftward shifted as compared to the other two pitch values. Thus, the pitch of 5 mm (Ratio = 0.4) gives the highest HTC, though the pitches of 5.5 mm (Ratio = 0.36) and 4.5 mm (Ratio = 0.44) also have greater HTC compared to the plain surface (Ratio = 0) (Figure 12a). Figure 12b shows the enhancement percentage in HTC of different pitch surfaces as compared to that of the Surface-P (Ratio = 0) at different specific heat fluxes. The enhancement percentage of HTC shows that the degradation with the rise in heat flux is due to the commencement of the nucleate boiling on the Surface-P at a specific heat flux.

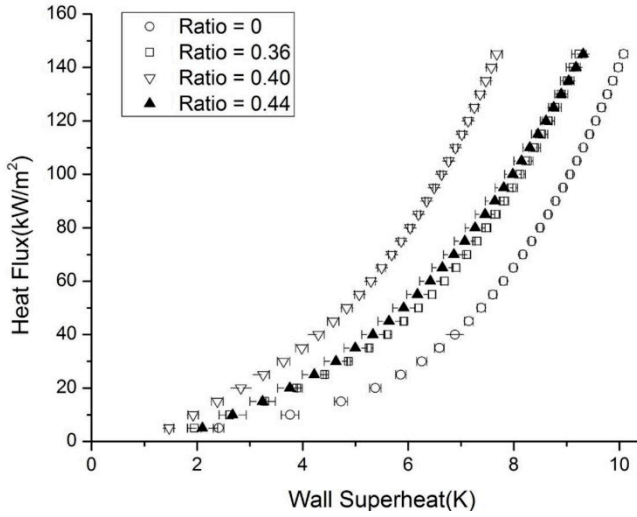

Figure 11. The effect of the pitch on the pool boiling curves of the various tested surfaces.

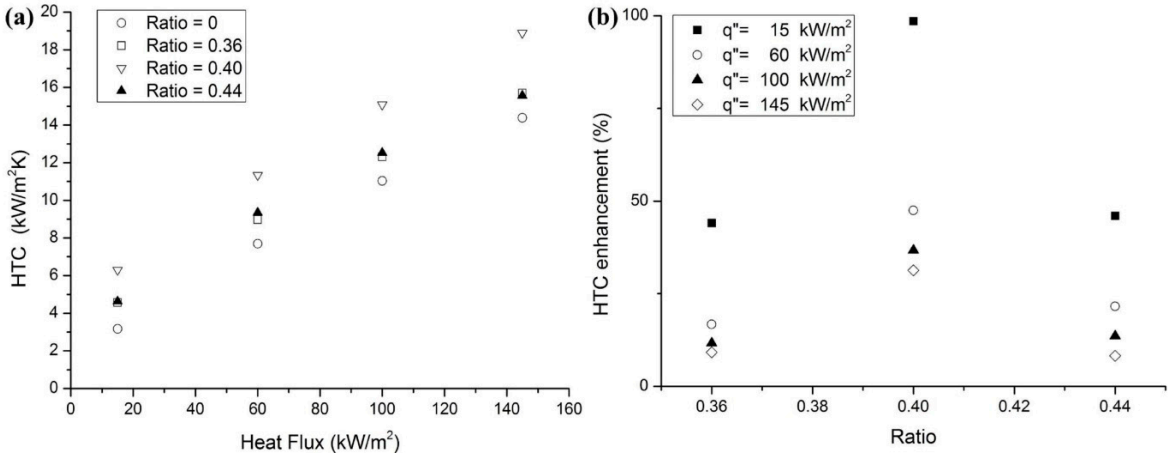

Figure 12. The effect of the pitch on (**a**) the HTC values for the specific heat fluxes and (**b**) the enhancement percentage in HTC with respect to the heat flux.

For the pitch of 5.5 mm (Ratio = 0.36), the merging chance of inter coalescence is reduced (Figure 13a). In contrast, for the pitch of 4.5 mm (Ratio = 0.44) (Figure 13b) and 5 mm (Ratio = 0.4) (Figure 10c), two types of the bubble coalescences occur on the heated surface. From the experimental results, we can infer that the effect of the pitch dominates in this case. In addition, the ratio of the hydrophobic area to the heating area seems to be an insignificant parameter on boiling heat transfer performance.

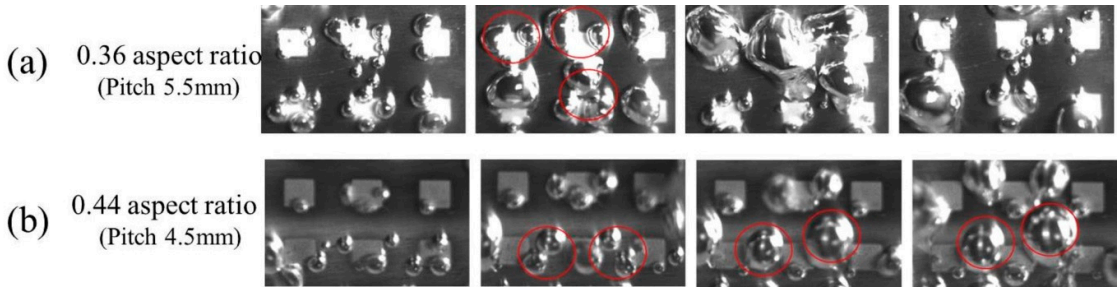

Figure 13. Bubble development mechanisms of the surfaces with (**a**) 0.36 aspect ratio and (**b**) 0.44 aspect ratio.

It appears that the inter coalescence of bubbles on the heated surface in the axial direction at the earlier stage of development is not beneficial for boiling heat transfer due to the increase in the bubble contact resistance [19]. This is because of the stop in the supply of replenishing liquid on the surface, resulting from the earlier merged bubbles (Figure 5a). Thus, the inter-distance should be sufficient to keep the continuous flow of replenishing liquid and to prevent the earlier stage of bubble merging on the copper in the axial direction (Figure 5b).

The departure diameter of the bubble from the interface of the pattern is shown in Figure 14a, and the observed value is 2.35 $\pm$ 0.03 mm. Subsequently, we estimated the minimum distance between the patterns for avoiding early inter coalescence of bubbles graphically by assuming the bubbles formed on the interline between the hydrophobic pattern and plain copper. The value of departure diameter is taken from the information given by the recorded image (Figure 14a). The estimated minimum inter-distance between the patterns is about 3.12 mm as shown in Figure 14b, which means that an inter-distance below this value will have a chance to allow for an earlier inter coalescence of bubbles in the axial direction. In addition, the cases in which the inter-distance is close to the estimated value will give the advantage of the axial inter coalescence without the early bubble merging on the copper. Therefore, the best design is the 2 mm sized square pattern (Ratio = 0.4) with a pitch of 5 mm (inter-distance = 3 mm), which results in superior heat transfer performance compared to other options tested.

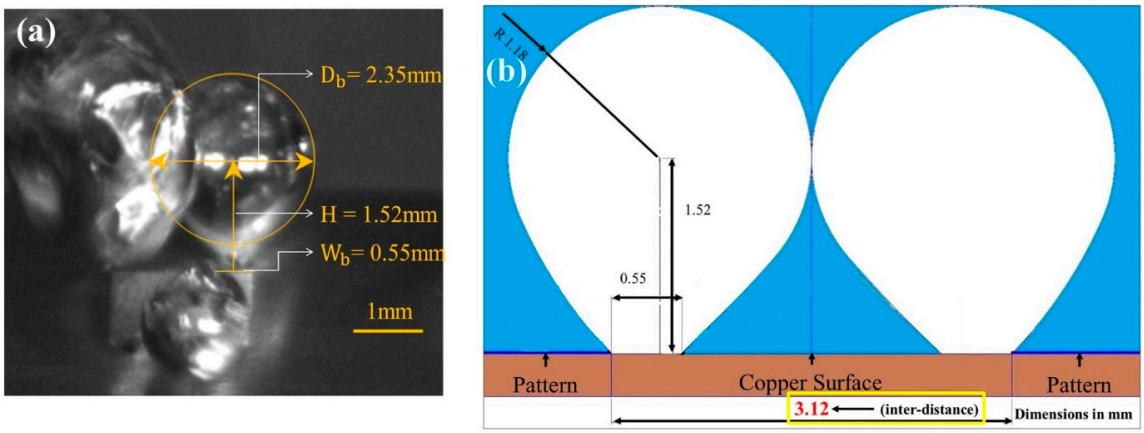

Figure 14. (**a**) Measured bubble departure size at the interface of the pattern and copper and (**b**) the minimum graphically estimated patterns.

4. Conclusions

In this work, the heterogeneous wettable surfaces were prepared by screen printing the hydrophobic polymer mixture on the plain hollow copper test pieces. The pool boiling heat transfer

performance of the different heterogeneous wettable surfaces was experimentally investigated by using the saturated water as the working fluid. The results are summarized as follows:

1. Three types of the development behaviors were observed on the heterogeneous wettable surfaces: the isolated development of a bubble, the internal coalescence of bubbles, and the inter coalescence of bubbles in the axial and circumferential directions. The isolated bubble development had a longer departure time and was most frequent at low heat fluxes. However, internal and inter coalescences in the circumferential direction took less departure time due to the influence of the merging of the bubbles.
2. The 2 mm size square pattern (Ratio = 0.4) produced a superior pool boiling heat transfer performance compared to all other aspect ratios studied. This is due to the presence of more bubbles at the interfaces, internal coalescence, the inter coalescence in the circumferential direction, and the inter coalescence of bubbles in the axial direction at the time of departure. Therefore, the 2 mm size square pattern (Ratio = 0.4) is the best design.

Supplementary Materials: Supplementary materials can be found at www.mdpi.com/2411-5134/3/1/15/s1.

Acknowledgments: The authors gratefully acknowledge funding support from the Ministry of Science and Technology, MOST (project numbers: MOST 104-2218-E-002-004, MOST 105-2218-E-002-019, MOST 105-2221-E-002-107-MY3, MOST 102-2221-E-002-133-MY3, and MOST 102-2221-E-002-088-MY3).

Author Contributions: Sujith Kumar C. S., Yao Wen Chang, conceived and designed the experiments; Sujith Kumar C. S., Yao Wen Chang and Yu Hsuan Chuang performed the experiments; Sujith Kumar C. S., Yao Wen Chang, Mario R. Mata Arenales, and Long-Sheng Kuo analyzed the data; Sujith Kumar C. S. wrote the paper; and Ping-Hei Chen guided through out the work.

Conflicts of Interest: The authors declare no conflict of interest.

References

1. Shen, B.; Yamada, M.; Hidaka, S.; Liu, J.; Shiomi, J.; Amberg, G.; Do-Quang, M.; Kohno, M.; Takahashi, K.; Takata, Y. Early Onset of Nucleate Boiling on Gas-covered Biphilic Surfaces. *Sci. Rep.* **2017**, *7*, 2036. [CrossRef] [PubMed]
2. Dhillon, N.S.; Buongiorno, J.; Varanasi, K.J. Critical heat flux maxima during boiling crisis on textured surfaces. *Nat. Commun.* **2015**, *6*, 8247. [CrossRef] [PubMed]
3. O'Hanley, H.; Coyle, C.; Buongiorno, J.; McKrell, T.; Hu, L.; Rubner, M.; Cohen, R. Separate effects of surface roughness, wettability, and porosity on the boiling critical heat flux. *Appl. Phys. Lett.* **2013**, *103*, 024102. [CrossRef]
4. Garimella, S.V.; Fleischer, A.S.; Murthy, J.Y.; Keshavarzi, A.; Prasher, R. Thermal Challenges in Next-Generation Electronic Systems. *IEEE Trans. Adv. Packag.* **2008**, *31*, 801–815. [CrossRef]
5. Lienhard, J.H., IV; Lienhard, J.H., V. *A Heat Transfer Textbook*, 3rd ed.; Phlogiston Press: Cambridge, UK, 2008.
6. Dharmendra, M.; Suresh, S.; Kumar, C.S.S.; Yang, Q. Pool Boiling Heat Transfer enhancement using vertically aligned Carbon Nanotube Coatings on a copper substrate. *Appl. Therm. Eng.* **2016**, *99*, 61–71. [CrossRef]
7. Boudouh, M.; Gualous, H.L.; de Labachelerie, M. Local convective boiling heat transfer and pressure drop of nanofluid in narrow rectangular channels. *Appl. Therm. Eng.* **2010**, *30*, 2619–2631. [CrossRef]
8. Kottoff, S.; Gorenflo, D.; Danger, E.; Luke, A. Heat transfer and bubble formation in pool boiling: Effect of basic surface modifications for heat transfer enhancement. *Int. J. Therm. Sci.* **2006**, *3*, 217–236. [CrossRef]
9. El-Genk, M.S.; Ali, A.F. Enhanced nucleate boiling on copper micro-porous surfaces. *Int. J. Multiph. Flow* **2010**, *36*, 780–792. [CrossRef]
10. Kumar, C.S.S.; Suresh, S.; Yang, L.; Yang, Q.; Aravind, S. Flow boiling heat transfer enhancement using carbon nanotube coatings. *Appl. Therm. Eng.* **2014**, *65*, 166–175. [CrossRef]
11. Phan, H.T.; Caney, N.; Marty, P.; Colasson, S.; Gavillet, J. How does Surface Wettability Influence Nucleate Boiling? *CR Mécanique* **2009**, *337*, 251–259. [CrossRef]
12. Wen, R.; Li, Q.; Wang, W.; Latour, B.; Li, C.H.; Li, C.; Lee, Y.; Yang, R. Enhanced Bubble Nucleation and Liquid Rewetting for Highly Efficient Boiling Heat Transfer on Two-level Hierarchical Surfaces with Patterned Copper Nanowire Arrays. *Nano Energy* **2017**, *38*, 59–65. [CrossRef]

13. Jo, H.-J.; Ahn, H.S.; Kang, S.-H.; Kim, M.H. A Study of Nucleate Boiling Heat Transfer on Hydrophilic, Hydrophobic and Heterogeneous Wetting Surfaces. *Int. J. Heat Mass Transf.* **2011**, *54*, 5643–5652. [CrossRef]
14. Choi, C.-H.; David, M.; Gao, Z.; Chang, A.; Allen, M.; Wang, H.; Chang, C.-H. Large-scale Generation of Patterned Bubble Arrays on Printed Bi-functional Boiling Surfaces. *Sci. Rep.* **2016**, *6*, 23760. [CrossRef] [PubMed]
15. Kumar, C.S.S.; Chang, Y.W.; Chen, P.H. Pool Boiling Heat Transfer Enhancement on Cylindrical Surfaces with Hybrid Wettable Patterns. *J. Vis. Exp.* **2017**, *122*. [CrossRef] [PubMed]
16. Huang, D.J.; Leu, T.Z.-S. Fabrication of high wettability gradient on copper substrate. *Appl. Surf. Sci.* **2013**, *280*, 25–32. [CrossRef]
17. Hsu, C.C.; Lee, M.R.; Wu, C.H.; Chen, P.H. Effect of interlaced wettability on horizontal copper cylinders in nucleate pool boiling. *Appl. Therm. Eng.* **2017**, *112*, 1187–1194. [CrossRef]
18. Taylor, J.R. *An Introduction to Error Analysis: The Study of Uncertainties in Physical Measurements*, 2nd ed.; University Science Books: Sausalito, CA, USA, 1997.
19. Rahman, M.M.; Pollack, J.; McCarthy, M. Increasing boiling heat transfer using low conductivity materials. *Sci. Rep.* **2015**, *5*, 13145. [CrossRef] [PubMed]
20. Kumar, C.S.S.; Chang, Y.W.; Chen, P.H. Effect of heterogeneous wettable structures on pool boiling performance of cylindrical copper surfaces. *Appl. Therm. Eng.* **2017**, *127*, 1184–1193. [CrossRef]